Available online at www.sciencedirect.com
ScienceDirect
Ultramicroscopy 107 (2007) 414–421
ultramicroscopy
www.elsevier.com/locate/ultramic

Many-beam dynamical simulation of electron backscatter diffraction patterns

Aimo Winkelmann[a,*], Carol Trager-Cowan[b], Francis Sweeney[b], Austin P. Day[c], Peter Parbrook[d]

[a] *Max-Planck-Institut für Mikrostrukturphysik, Weinberg 2, D-06120 Halle, Germany*
[b] *Department of Physics, University of Strathclyde, Glasgow G4 ONG, Scotland, UK*
[c] *Aunt Daisy Scientific Ltd., Dixton Rd., Monmouth, Gwent, NP25 3PP, UK*
[d] *EPSRC National Centre for III–V Technologies, University of Sheffield, UK*

Received 9 July 2006; received in revised form 4 October 2006; accepted 17 October 2006

Abstract

We present an approach for the simulation of complete electron backscatter diffraction (EBSD) patterns where the relative intensity distributions in the patterns are accurately reproduced. The Bloch wave theory is applied to describe the electron diffraction process. For the simulation of experimental patterns with a large field of view, a large number of reflecting planes has to be taken into account. This is made possible by the Bethe perturbation of weak reflections. Very good agreement is obtained for simulated and experimental patterns of gallium nitride GaN{0 0 0 1} at 20 kV electron energy. Experimental features like zone-axis fine structure and higher-order Laue zone rings are accurately reproduced. We discuss the influence of the diffraction of the incident beam in our experiment.
© 2006 Elsevier B.V. All rights reserved.

PACS: 61.14.−x

Keywords: Electron backscatter diffraction

1. Introduction

Electron backscatter diffraction (EBSD) has developed into a valuable tool for the analysis of crystalline materials [1].

This technique, which is based around the scanning electron microscope (SEM), uses a highly tilted specimen which points towards the scintillating screen of an EBSD detector. A schematic picture of this is shown in Fig. 1. When the stationary electron beam strikes the specimen, the electrons backscattered from the sample produce a diffraction pattern on the phosphor screen. A high sensitivity, low-light level CCD camera is used to view the phosphor and to capture an image of the electron backscatter pattern (EBSP).

An EBSP consists of a series of overlapping Kikuchi bands. The edges of each Kikuchi band correspond to diffraction from opposite sides of the same set of planes within the crystal. In presently existing commercial software, dedicated image analysis and indexing algorithms are used to identify the orientation of the crystal that would produce the corresponding diffraction pattern. By automating the movement of the electron beam or stage in the SEM, it is possible to produce maps that show variations in crystallographic orientation and phase across an area of the specimen.

The main advantages of the EBSD technique are that it has high spatial resolution, of the order of 20 nm in a Schottky field emission SEM, and it allows the local crystallography to be measured and directly compared with the microstructure. In addition, it is possible to tune the depth sensitivity by the choice of the electron energy.

Applications of EBSD include measurement of texture, grain size and phase distribution. With the combination of high-quality EBSPs, chemical data from X-ray fluorescence measurements, and suitable crystallographic databases, it is

*Corresponding author. Tel.: +49 345 5582639; fax: +49 345 5511223.
E-mail address: winkelm@mpi-halle.mpg.de (A. Winkelmann).

0304-3991/$ - see front matter © 2006 Elsevier B.V. All rights reserved.
doi:10.1016/j.ultramic.2006.10.006

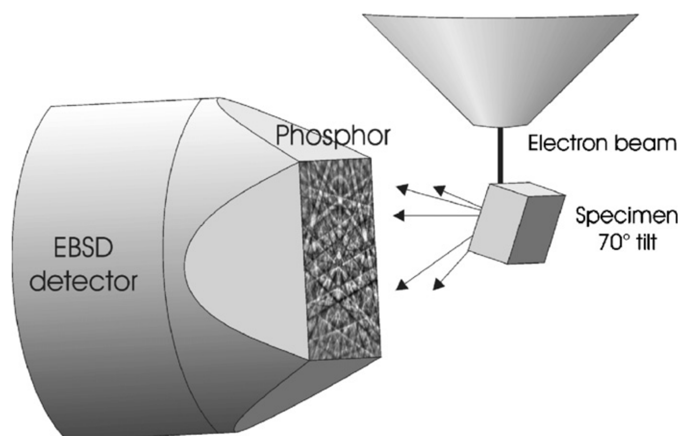

Fig. 1. Schematic showing the EBSD geometry used in this work.

possible to perform phase identification and crystal symmetry determination [2]. EBSD has also been applied to the measurement of local elastic strain and small rotations [3].

Most commercial EBSD systems use the Bragg equation, $n\lambda = 2d \sin \theta$, to predict the positions of the Kikuchi band edges and the kinematical diffraction model to estimate the relative intensities of the Kikuchi bands [1,4]. The Hough transform [1,5] is used to detect the Kikuchi bands, the angles between the corresponding crystal planes are used as a key to match against the theoretical interplanar angles. For this reason, it is essential to have accurate crystallographic data (including atom position information) for the phases to be analyzed.

There is significant information contained in the complicated intensity distributions of the EBSPs. Pronounced improvements in applications of the EBSD method can be expected if it is possible to gain access to a quantitative description of EBSD patterns and hence extract the information provided by intensity variations in the EBSPs. The continuous improvement of the experimental technique has resulted in observable fine-structure effects in the patterns which call for a comparison with such quantitative simulations.

A complete simulation of the observed intensities is only possible by applying the dynamical theory of electron diffraction which properly includes the effects of multiple scattering in the crystal. This theory is well developed and used extensively in various areas of electron diffraction for the analysis of experimentally observed effects [6,7].

In this paper, we present results of an attempt to simulate the relative intensity distributions of complete backscatter patterns which can be used for thin film crystallography. Our first results focus on the reproducibility of experimental patterns from gallium nitride. We will show that by the application of our approach, the experimental patterns can be very nicely reproduced. We have to stress that we do not attempt quantitative agreement in intensities, but rather it is our aim to show how much of the complicated relative intensity distribution can be explained by taking into account all possible diffracting planes and their interaction in dynamical scattering. The results will be displayed as a two-dimensional map emphasizing the structures in the diffraction pattern and their relative intensities comparable to the approach described in the paper of Rossouw et al. [8] with the additional inclusion of geometrical effects in our setup.

2. Experiment

The experimental EBSPs were taken using a Nordlys II detector with CHANNEL 5 software (HKL technology) on a Carl Zeiss Supra 55VP FEGSEM. For EBSD work, the lateral spatial resolution is of the order of tens of nm. The 1600 nm GaN sample was grown by metalorganic vapor phase epitaxy using a Thomas Swan Showerhead reactor. A 30 nm GaN nucleation layer was first grown at 525 °C on a (0 0 0 1) sapphire substrate. This nucleation layer was then annealed briefly at a GaN growth temperature of 1023 °C prior to thin film growth. The sample was mounted on an aluminum stub, tilted to $\approx 70^\circ$ from the horizontal and positioned below the electron beam at a working distance of 8 mm. The accelerating voltage was 20 kV, the probe current was about 1 nA. The Nordlys detector was inserted 176 mm into the SEM chamber providing a phosphor-to-sample distance of 19 mm. All patterns were taken at room temperature; however, the effects of localized heating due to the electron beam are unknown. The incoming beam direction was estimated to be near the $[\bar{1}\,3\,\bar{2}\,1]$ direction. Because a flat phosphor screen is used in the detection of the EBSPs, the observed patterns are given in a gnomonic projection.

3. Theory

Our approach is a straightforward application of the Bloch wave theory of electron diffraction which describes the diffraction of an electron plane wave by a crystal lattice. The crystal lattice acts as a very complicated diffraction grating where electrons are focused to different positions inside the crystal. Depending on the incidence angle of an incoming plane wave relative to the lattice planes, the diffracted electrons interact differently with the atoms which constitute the crystal. This effect for instance causes the incoming electrons to penetrate the crystal along certain directions further than along others. Pictorially, this has been termed as “channeling”, but one should keep in mind that in general one has to deal with a diffraction effect which modulates the probability of inelastic processes. Manifestations of this can be observed as an angular dependence of a number of inelastic processes which happen during the diffraction of the incident beam, for instance the production of Auger electrons, X-rays, and backscattered electrons. If the latter are observed as a function of the incidence angle in a SEM, one obtains the electron channeling patterns (ECP).

ECP are closely related to EBSD [9]. The reciprocity principle states that the observed intensity at a point detector inside the sample, after diffraction of an incoming plane wave, is the same as for a detected plane wave intensity after diffraction of waves emanating from a point source inside the sample. This powerful principle has a large number of applications in electron diffraction theories, because it restates the difficult problem of spherical waves emanating from point sources to the conceptually simpler picture of a diffracted plane wave [10]. In this way, the dominant diffraction process in EBSD (outgoing beam diffraction) and ECP (incident beam diffraction) can be described by exactly the same mathematical formalism. This does not mean that EBSD and ECP are the exact reciprocal versions of each other. They both emphasize different parts of a more general process containing incident beam diffraction, inelastic scattering, and outgoing diffraction.

Theories for the observed intensities in ECP have been presented by Hirsch and Humphreys [11], Vicario et al. [12] and Reimer et al. [13]. A large number of the investigations were driven by the need to understand the diffraction contrast of lattice defects [14,15]. Many-beam effects in ECP have been studied before by Marthinsen [16–18]. Further simulations were done by Rossouw [8] using a dependent Bloch wave model and Dudarev [19] using an inhomogeneous transport equation approach for the inelastically scattered electrons.

The model that is used for our EBSD simulations is schematically summarized in Fig. 2. An incident beam with a certain angular divergence is impinging on the sample and diffracted to produce a modified distribution of the incoming electrons relative to the atoms of the crystal. This diffracted electron distribution undergoes an inelastic process, in our case the quasi-elastic backscattering from the atomic nucleus. The backscattered electrons are thought to originate with the energy of the incident beam from point sources inside the crystal and are then subject to the diffraction process by the surrounding crystal lattice. The source strength for this outgoing diffraction is determined by the cross-section of the inelastic process under consideration. We also assume that the inelastic process destroys the coherence, and in this approximation the incoming and outgoing diffraction processes do not interfere. For the case of quasi-elastic backscattering, it is shown in Fig. 2 that Ga has a much larger cross-section than N. Thus the electrons backscattered from Ga dominate the EBSP if the relative intensity incident on N and Ga atoms clearly differs less than the inelastic cross-sections. This means that if the incident beam cannot produce a large enough difference of the incoming electrons on Ga and N atoms, the final intensity will always be dominated by the stronger backscattering on Ga alone and any effects due to the diffraction of the incoming beam will be reduced. In this approximation, diffraction of the incident electron beam and inelastic transport effects can be assumed to have a minor influence on the final backscattering pattern, also considering the geometrical setup of the experiment [9]. For the case of GaN, we discuss the influence of the incident beam diffraction and attenuation in Section 4.

Our assumption of quasi-elastic scattering clearly is very simplified, because also inelastically scattered electrons with larger energy losses contribute to the EBSP. Ideally, a number of EBSP for different energies would have to be calculated and summed according to their spectral weight. This will have the main effect of blurring the diffraction features in the experimental patterns as compared to simulations at a fixed energy. As long as the spectrum of inelastically scattered electrons is dominated by electrons

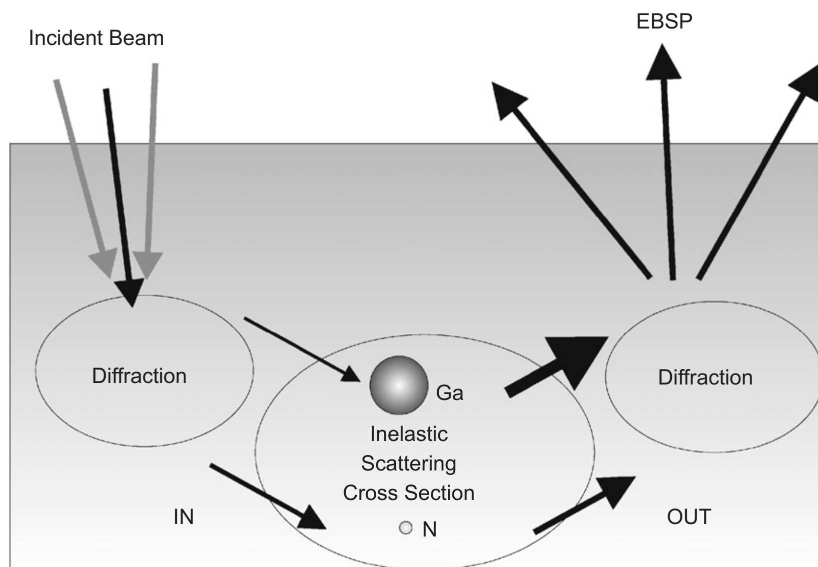

Fig. 2. Schematic model applied for the simulation.

within a small enough energy range, the approximation of a single fixed energy should be reasonable. Thereby the size of the computation is considerably reduced.

In the general case for arbitrary incidence and takeoff angles, the effects of multiple inelastic scattering, for instance, can lead to a contrast reversal of the Kikuchi bands [9]. We have to stress that while a complete theory has to take into account the inelastic transport effects, our approach will reveal the effects for which basically the many-beam diffraction processes are responsible.

The reciprocity principle allows us to use the framework of previous ECP simulations also for EBSD [20,21]. A Bloch wave approach is used to describe the diffraction of electrons with wavevector $\mathbf{k}_0$. The use of this method is described in several reviews [6,7], the following is a short summary.

The wavefunction inside the crystal is described as a superposition of Bloch waves with wavevectors $\mathbf{k}^{(j)}$

$$\Psi(\mathbf{r}) = \sum_j c_j \exp(\mathrm{i}\mathbf{k}^{(j)} \cdot \mathbf{r}) \sum_{\mathbf{g}} C_{\mathbf{g}}^{(j)} \exp(\mathrm{i}\mathbf{g} \cdot \mathbf{r}). \quad (1)$$

One introduces the total (scaled) potential $U(\mathbf{r})$:

$$U(\mathbf{r}) = U^c(\mathbf{r}) + \mathrm{i}U'(\mathbf{r}) = \sum_{\mathbf{g}} U_{\mathbf{g}} \exp(\mathrm{i}\mathbf{g} \cdot \mathbf{r}). \quad (2)$$

The potential is described by complex electron structure factors $U_{\mathbf{g}}^c = 2mV_{\mathbf{g}}/\hbar^2$ with $V_{\mathbf{g}}$ being a Fourier coefficient of the crystal potential in eV and the relativistic electron mass m. The loss of electrons from the initial population due to inelastic effects is included by the definition of the imaginary components $U'_{\mathbf{g}}$.

Substitution of these expressions for the wavefunction and the potential into the Schrödinger equation leads to the standard dispersion relation

$$[\mathbf{K}^2 - (\mathbf{k}^{(j)} + \mathbf{g})^2]C_{\mathbf{g}}^{(j)} + \sum_{\mathbf{h}} U_{\mathbf{g}-\mathbf{h}} C_{\mathbf{h}}^{(j)} = 0, \quad (3)$$

where $\mathbf{K}$ is the electron wavevector inside the crystal, $k_0^2 = K^2 - U_0^c$.

Then $\mathbf{k}^{(j)}$ is written as

$$\mathbf{k}^{(j)} = \mathbf{K} + \lambda^{(j)}\mathbf{n}, \quad (4)$$

where $\mathbf{n}$ is a unit vector normal to the surface. One can then transform (3) into an eigenvalue problem [7] which gives the eigenvalues $\lambda^{(j)}$ and eigenvectors with elements $C_{\mathbf{g}}^{(j)}$. This includes the effects due to the tilt of the outgoing direction to the surface [22] and is valid for reciprocal space vectors $\mathbf{g}$ also in higher-order Laue zones (HOLZ).

The boundary conditions at the surface determine the coefficients c_j in (1). These quantities are given by the elements of the first column of the inverse of the matrix whose elements are $C_{\mathbf{g}}^{(j)}$ [7]. After this, the wavefunction (1) is known and can be used to calculate the electron probability density inside the crystal.

The Fourier coefficients $V_{\mathbf{g}}$ of the real part of the crystal potential can be calculated from the contributions of the atoms which constitute the unit cell:

$$V_{\mathbf{g}} = \frac{1}{\Omega} \sum_i f_i^e(s) \exp(-\mathrm{i}\mathbf{g} \cdot \mathbf{r}_i) \quad (5)$$

with the atoms at positions $\mathbf{r}_i$ in the unit cell volume Ω and the Fourier coefficients $f^e(s)$, $s = |\mathbf{g}|/2$ of the atomic potentials. The $f^e(s)$ can be calculated from parameters tabulated in the literature by Doyle and Turner [23] or taken from other available parametrizations [24,25]. For the imaginary part of the potential we used the absorptive form factor parameters of Weickenmeier et al. [25] which were calculated using an Einstein model for the lattice vibrations.

The eigenvalue method described above scales as N^3 with the number N of the included reflecting planes. This quickly leads to impractically long computation times if a large number of reflections has to be included. This can be overcome by the use of the Bethe perturbation scheme [7] which allows the inclusion of the effects of weak reflections $U_{\mathbf{h}}$ by the transformation into an effective potential of the strong beams $U_{\mathbf{g}}^{\text{eff}}$ without increasing the matrix dimensions:

$$U_{\mathbf{g}}^{\text{eff}} = U_{\mathbf{g}} - \sum_{\mathbf{h}} \frac{U_{\mathbf{h}} U_{\mathbf{g}-\mathbf{h}}}{2KS_{\mathbf{h}}}, \quad (6)$$

where $2KS_{\mathbf{h}}$ is defined by $2KS_{\mathbf{h}} = K^2 - (\mathbf{K} + \mathbf{h})^2$, containing the excitation error $S_{\mathbf{h}}$. For the use of the Bethe perturbation, beam selection and convergence criteria have been developed in the context of convergent beam electron diffraction [26,27]. Strong and weak beams are selected according to their structure factor and the excitation error, describing how strong the influence of a certain reflecting plane is at the considered point in the diffraction pattern. In our case, we have tested the convergence of this approach by comparing sets of perturbational simulations with calculations solving the full eigenvalue problem.

Finally, to compute the probability of electrons to be at the position of the backscattering nuclei, one has to calculate $\psi\psi^*$ from Eq. (1) [22]. The interaction of diffracted electrons with the crystal can be modeled by generalized potentials [28,29]. In the case that these potentials have the form of delta functions (point sources or point detectors) which are broadened by thermal vibrations, Rossouw et al. [8] have given the following expression for the depth integrated dynamically backscattered intensity from the crystal:

$$I_{\text{DYN}} \propto \sum_{n,ij} Z_n^2 B^{ij}(t) \sum_{\mathbf{g},\mathbf{h}} C_{\mathbf{g}}^{(i)} C_{\mathbf{h}}^{(j)*} \times \exp(-M_{\mathbf{g}-\mathbf{h}}^n) \exp[\mathrm{i}(\mathbf{g} - \mathbf{h}) \cdot \mathbf{r}_n] \quad (7)$$

with atoms at $\mathbf{r}_n$, Debye–Waller factors $\exp(-M_{\mathbf{g}-\mathbf{h}}^n)$ and a depth integrated interference term $B^{ij}(t)$ of the Bloch waves i and j:

$$B^{ij}(t) = c_i c_j \frac{\exp[\mathrm{i}(\lambda^i - \lambda^{j*})t] - 1}{\mathrm{i}(\lambda^i - \lambda^{j*})}. \quad (8)$$

Because the wave functions are known to be of the form in Eq. (1), the thickness integration can be carried out analytically. To the dynamical term has to be added a kinematical part which represents a plane-wave contribution to the backscattered intensity due to dechanneled electrons:

$$I_{\mathrm{KIN}} \propto \sum_{n} Z_n^2 \left(1 - \sum_{ij} B^{ij}(t) \sum_{\mathbf{g}} C_{\mathbf{g}}^{(i)} C_{\mathbf{g}}^{(j)*} \right). \quad (9)$$

In our calculation, the parameter t corresponds to the thickness of the film along the surface normal, the varying thickness for different outgoing directions is taken into account into the definition of the initial eigenvalue problem (see above). The relative intensity distribution will not very sensitively depend on this parameter since it produces only large angular range intensity variations.

Using the method described above, the backscattering pattern can be calculated point by point, each describing a well-defined wavevector direction $\mathbf{k}_0$. The application of the Bethe perturbation scheme allows the inclusion of a large number of reflecting planes so that the large viewing angles in EBSD can be handled. For comparison with the experimental patterns, the calculation has to be rescaled according to the gnomonic projection used in the experiment.

While the model described is conceptually simple, so far there have not been simulations which can take into account the large number of lattice planes necessary to describe the dynamical fine structure in the patterns.

4. Results

4.1. Parameters

For the calculation of the GaN backscattering pattern, more than 1200 reflections with a minimum lattice spacing $d_{hkl} = 0.5\,\text{Å}$ have been taken into account. This set of lattice planes was generated by an automatic beam setup routine which can select reflecting planes due to their scattering strength (structure factor), their lattice spacing or whether they belong to a specified (higher order) Laue zone. The lattice constants for GaN in the wurtzite structure were assumed as $c = 5.178$ and $a = 3.189\,\text{Å}$. The Debye–Waller factor was taken from Yoshiasa et al. [30].

4.2. Incident beam diffraction

First, we discuss the influence of the diffraction of the incoming beam in our experimental geometry. Because the incoming beam direction is not known exactly, we need an estimation of the influence of this parameter on the final intensity variation. This is especially important for samples containing different kinds of atoms. The final EBSP is the sum of the backscattered intensity from all atoms in the unit cell. In this sense, each atom of the unit cell produces its own "element-resolved" EBSP. If the unit cell contains atoms which differ in their local crystallographic environment, the EBSP produced by each element will also differ. With a change of the diffraction of the incoming beam, the number of electrons diffracted to each of these atomic sites can change and thus their relative contribution to the final EBSP. We will show that in our case the Ga atoms are usually the most relevant in the end because of their much larger backscattering cross-section.

An estimation of the upper limit of the relative magnitude of the diffraction of the incoming beam comes from the analysis of the intensity variations in the diffraction features of the experimental backscattering pattern. By reciprocity, a hypothetical *incident* beam would be able to produce only variations of roughly this magnitude at the backscattering atoms. From a histogram analysis of the experimental backscattering pattern, we find that typically for 95% of the incident directions analyzed the intensity variations are within a factor of 0.5–1.5 from the average value. This already illustrates that without a very accurate setting of the incident beam direction it is very unlikely that large effects due to the diffraction of the incoming beam will be discernible.

To analyze this also theoretically, we show in Fig. 3 the calculated element resolved intensity at the Ga and N atoms due to the diffraction of a plane wave with the energy of the incident electrons (20 kV). This calculation is equivalent to a simulation of element resolved ECP. Using a spherical projection, we show how much intensity is present at the lattice sites of Ga and N, respectively, after diffraction of the incoming beam with a direction in the quadrant plotted. The patterns shown are a fourth of the full hemisphere above the sample and each point corresponds to a specific incident beam direction with polar angles up to 80°, which mark the border of the circular area. The surface normal direction {0 0 0 1} is located in the lower left corner of the figures. The lower panel of Fig. 3 shows the ratio between the intensity diffracted to the N atoms and the intensity diffracted to the Ga atoms. For 95% of the incident beam directions, the ratio N/Ga of the relative intensities at the N and Ga atoms is between a factor of 0.4–2.5. Thus the simulation predicts a higher influence of the incident beam diffraction than estimated from the experiment. This is not surprising since we assumed a perfect parallel beam in the simulation. Nevertheless, the order of magnitude of the predicted effect is comparable to the experimental estimation.

The much heavier Ga atoms usually have the most influence on the final diffraction pattern, due to the Z^2 dependence of the backscattering cross-section. Ga backscatters almost 20 times more than N for equal incident intensities. So even if we assume that we have a perfect plane wave incident beam and our incident direction is near one of the very specific diffraction directions where the N/Ga incident ratio is exceptionally high (say 4), after backscattering there will be 20 parts for Ga and 4 parts for N, which means even in this situation, the N atom

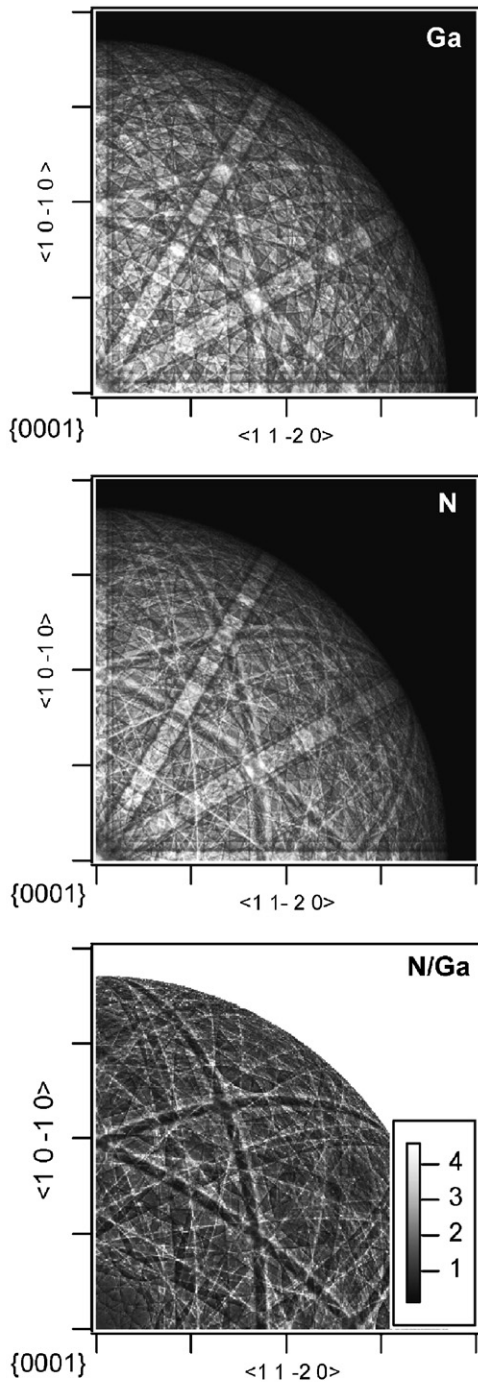

Fig. 3. Incident beam diffraction: element resolved intensities in GaN{0 0 0 1} at 20 kV, top: Ga, middle: N. The data shown is drawn according to a spherical projection with the maximum polar angle of 80°. The surface normal direction {0 0 0 1} corresponds to the lower left corner of each graph. The lower panel shows the ratio between the integrated intensities near Ga and N atoms.

diffraction pattern will still only contribute less than 20% to the final EBSP. For a beam with a certain angular divergence which is not incident along one of the special directions, this value will become much less. We thus have good reason to assume that the ratio of backscattered intensity from Ga and N will usually be dominated by Ga for our experimental conditions if no special measures are applied to enhance the incident beam diffraction effect. It is thus not surprising that our experimental EBSP are still very well described by neglecting the incident beam diffraction influence in the simulation. That is why in the following we assume that the incoming beam direction as well as the probe convergence and incoherence are sufficient for the observed EBSD pattern not to be dominated by fine structure effects of the incoming beam diffraction, e.g. an exceptionally high N/Ga intensity ratio in certain directions.

Fig. 3 also illustrates how much information is lost due to the fact that EBSD is not element sensitive, because the pattern from N is quite different from the Ga pattern. If we turn our argument around, use of these differences could possibly be made for polarity determination by selective excitation and detection along special directions where the N/Ga ratio is increased due to diffraction effects. This incoming beam diffraction effect on EBSD patterns is applied for instance in the method of electron channeling contrast imaging (ECCI) [2] by choosing a geometry of incoming and outgoing beam directions which allow the sensitive observation of lattice defects.

4.3. EBSD from GaN

We calculated the EBSD intensity under the assumption that the backscattered intensity from Ga and N is near the ratio of $Z_{\mathrm{Ga}}^2/Z_{\mathrm{N}}^2$. The calculated intensity was rescaled using a gnomonic projection according to the geometrical conditions in the experiment. Due to the nature of this projection, there is a pronounced loss of resolution in the bottom area of the simulation which mimics the behavior of the experimental pattern which is subject to the same effect.

On comparison of a measured and the simulated pattern for GaN{0 0 0 1} (Fig. 4), a very good agreement is evident between simulation and experiment. First of all, the Kikuchi line positions are correctly reproduced—a result which by itself could also be obtained by the much more simpler kinematic theory. However, in addition to the line positions, the intensity distribution is also predicted by the dynamical theory. The dynamical intensities are not always a simple summation of intensities from different reflections, instead dynamical scattering leads to interference terms producing more complicated features, like bright spots or rings, especially when two or more lines cross. We also stress that although kinematic theory is able to predict the angles between Kikuchi lines, at least the two-beam dynamical theory is necessary to predict the minimum in intensity of a cross-section of a Kikuchi band. This minimum is a function of the electron beam energy and the structure factors and in general does not coincide with the Bragg angle of the lattice planes under consideration. In addition, the higher-order systematic row reflections which show up as parallel lines near to the main Kikuchi bands, are correctly reproduced. The reduced contrast and

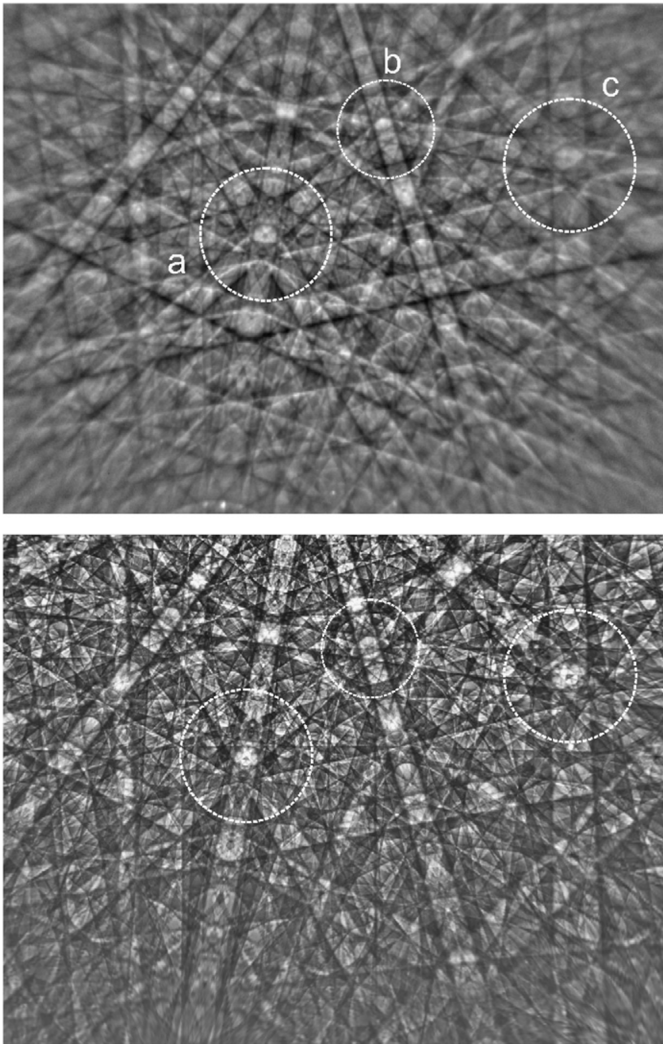

Fig. 4. EBSD of GaN{0 0 0 1} at 20 kV, top: experimental pattern, bottom: dynamical simulation. In area b, attention is drawn to the HOLZ ring at approximately $\frac{2}{3}$ of the radius of the area.

resolution in the experimental pattern as compared to the simulation are probably due to the neglect of multiple inelastic scatterings leading to a spread of the energies of the electrons producing the EBSP and a corresponding blurring of the diffraction features.

Because of the large number of features in the EBSD pattern, we draw attention to several selected regions of the pattern in Fig. 4. For instance, it can be seen that the fine structure in the zone axis regions (a) and (c) is strikingly similar in the two patterns. Because of strong dynamical interactions near a zone-axis, it is very important that our approach can reproduce the rather complicated intensity distribution near a zone axis. These intensities also show a pronounced energy dependence, even to the extent that they can be used as a fingerprint in identification of crystallographic phases [20,21].

In region (b) of Fig. 4, attention is drawn to the appearance of a HOLZ ring, which is located at about $\frac{2}{3}$ of region's (b) diameter. The increased intensity in this ring is related to decreased intensity at the position of dark HOLZ lines (deficient lines) near the zone axis [20]. Since the structure of these deficient lines is particularly sensitive to changes in lattice constants, obtaining more information by zooming in on this zone axis fine structure, by using a larger screen-to-sample distance for example, will certainly be a topic for future research.

Michael et al. [31] have analyzed the diameter of HOLZ rings observed in EBSD patterns. They found that dynamical effects cannot be disregarded. Our simulation by definition takes into account these dynamical effects and shows clear HOLZ rings for a number of zone axes, but some HOLZ rings in the simulated pattern do not appear as prominently as in the experiment. This may be due to the still limited number of lattice planes which have been taken into account. From the point of view of thin film crystallography, the diameter of HOLZ rings is related to the distance between atoms in a zone-axis direction. Single-scattering (real space) calculations and many-beam dynamical (reciprocal space) simulations have been used to demonstrate how the real space and the reciprocal space views of this diffraction process are connected in the closely related technique of photoelectron diffraction [32].

The observed fine structure is rather sensitive to the energy of the incoming electrons. In our calculations we saw noticeable changes in the pattern with a variation of 50 eV. In this way, the best fit between theory and experiment was found at 19.95 keV, as judged by visual inspection. Further investigations will focus on the energy dependence of the fine structure and the conclusions which can be drawn using this additional degree of freedom in the experiment.

Because the simulation very nicely reproduces all fine structure in the pattern, it shows that for further development of the EBSD method, the approach applied in this work represents a possible way to go. The quality of the simulated patterns directly implies their use as a fingerprint for phase identification. With the advantage of being able to include the gnomonic projection correctly, this greatly simplifies the procedure of comparison with experimental patterns.

5. Conclusion

In this paper, we have presented results of an attempt to simulate complete backscatter patterns which can be used for thin film crystallography. Our first results focused on the reproducibility of experimental patterns from gallium nitride. We showed that the experimental pattern can be very nicely reproduced by the application of the dynamical theory of electron diffraction and the use of the Bethe perturbational approach to solve the many-beam case, an approach which to our knowledge has not been previously taken for the simulation of EBSD. This opens the way for more quantitative analysis of EBSD patterns, with possible future applications in the fields of phase identification, determination of sample polarity, and the analysis of

HOLZ effects manifesting themselves in ring-structures and zone-axis fine structure. It will possibly also helpful in the development of methods for the determination of alloy compositions and to obtain a more detailed description of the channeling contrast of dislocations.

Our approach is a rather straightforward and conceptually simple implementation of the long-known and well-developed dynamical theory of electron diffraction for the case of EBSD with a very large number of reflections in arbitrary Laue zones. Necessary improvements include e.g. the handling of inelastic scattering processes and an improved description of the excitation process. We believe that quantitative simulations of experimental patterns are a prerequisite for further progress in the applications of EBSD. As has been the case in other fields of electron diffraction, the ability to compare simulated and experimental results should open up new ways for the interpretation of the wealth of information that is contained in the observed patterns.

Acknowledgments

This work was supported by the Royal Society of Edinburgh.

References

[1] A.J. Schwartz, M. Kumar, B.L. Adams (Eds.), Electron Backscatter Diffraction in Materials Science, Kluwer Academic/Plenum Publications, New York, 2000.
[2] A.J. Wilkinson, P.B. Hirsch, Micron 28 (1997) 279.
[3] A.J. Wilkinson, J. Electron Microsc. 49 (2) (2000) 299.
[4] N.H. Schmidt, N.O. Olsen, Can. Mineral. 27 (1989) 15.
[5] N.C. Krieger-Lassen, D. Jul-Jensen, K. Conradsen, Scanning Microsc. 6 (1992) 115.
[6] C.J. Humphreys, Rep. Prog. Phys. 42 (11) (1979) 1825.
[7] J.C.H. Spence, J.M. Zuo, Electron Microdiffraction, Plenum Press, New York, London, 1992.
[8] C.J. Rossouw, P.R. Miller, T.W. Josefsson, L.J. Allen, Philos. Mag. A 70 (6) (1994) 985.
[9] L. Reimer, Scanning Electron Microscopy—Physics of Image Formation and Microanalysis, Springer, Berlin, New York, 1998.
[10] M. von Laue, Materiewellen und ihre Interferenzen, Akademische Verlagsgesellschaft Geest & Portig, Leipzig, 1948.
[11] P.B. Hirsch, C.J. Humphreys, in: Proceedings of the Third Annual Scanning Electron Microscope Symposium, Chicago, IITRI Corporation, Chicago, 1970.
[12] E. Vicario, M. Pitaval, G. Fontaine, Acta Crystallogr. A 27 (1971) 1.
[13] L. Reimer, H.G. Badde, H. Seidel, W. Bühring, Z. Angew. Phys. 31 (1971) 145.
[14] J.P. Spencer, C.J. Humphreys, P.B. Hirsch, Philos. Mag. 26 (1972) 193.
[15] J.P. Spencer, C.J. Humphreys, Philos. Mag. A 42 (1980) 433.
[16] K. Marthinsen, R. Høier, Acta Crystallogr. A 42 (1986) 484.
[17] K. Marthinsen, R. Høier, Acta Crystallogr. A 44 (1988) 700.
[18] K. Marthinsen, R. Høier, Acta Crystallogr. A 44 (1988) 693.
[19] S.L. Dudarev, P. Rez, M.J. Whelan, Phys. Rev. B 51 (1995) 3397.
[20] A. Winkelmann, B. Schröter, W. Richter, Ultramicroscopy 98 (2003) 1.
[21] A. Winkelmann, B. Schröter, W. Richter, J. Phys. Condens. Matter 16 (2004) 1555.
[22] L.J. Allen, C.J. Rossouw, Phys. Rev. B 39 (12) (1989) 8313.
[23] P.A. Doyle, P.S. Turner, Acta Crystallogr. A 24 (1968) 390.
[24] D.M. Bird, Q.A. King, Acta Crystallogr. A 46 (1990) 202.
[25] A. Weickenmeier, H. Kohl, Acta Crystallogr. A 47 (1991) 590.
[26] J.M. Zuo, A.L. Weickenmeier, Ultramicroscopy 57 (1995) 375.
[27] C. Birkeland, R. Holmestad, K. Marthinsen, R. Hoier, Ultramicroscopy 66 (1996) 89.
[28] L.J. Allen, C.J. Rossouw, Phys. Rev. B 42 (18) (1990) 11644.
[29] L.J. Allen, C.J. Rossouw, Phys. Rev. B 47 (5) (1993) 2446.
[30] A. Yoshiasa, K. Koto, H. Maeda, T. Ishii, Jap. J. Appl. Phys. 36 (2) (1997) 781.
[31] J.R. Michael, J.A. Eades, Ultramicroscopy 81 (2000) 67.
[32] A. Winkelmann, B. Schröter, W. Richter, Phys. Rev. B 69 (24) (2004) 245417.